Electronic Supplementary Material (ESI) for Physical Chemistry Chemical Physics.

Supporting Information

Cyclic ion mobility of doped $[MAu_{24}L_{18}]^{2-}$ superatoms and their fragments (M = Ni, Pd and Pt; L = alkynyl).

Frank Hennrich[a,d], Shun Ito[b], Patrick Weis[a], Marco Neumaier[a,c], Shinjiro Takano[b], Tatsuya Tsukuda[b] and Manfred M. Kappes[a,b,d]

[a]Institute of Physical Chemistry, Karlsruhe Institute of Technology, Fritz-Haber-Weg 2, 76131 Karlsruhe, Germany.
[b]Department of Chemistry, Graduate School of Science, The University of Tokyo,7-3-1 Hongo, Bunkyo-ku, Tokyo 113-0033, Japan.
[c]Institute of Nanotechnology, Karlsruhe Institute of Technology, Hermann-von-Helmholtz-Platz 1, 76344 Eggenstein-Leopoldshafen, Germany.
[d] Institute of Quantum Technologies and Materials, Karlsruhe Institute of Technology, Hermann-von-Helmholtz-Platz 1, 76344 Eggenstein-Leopoldshafen, Germany.

Contents

Synthetic Methods

Materials

All solvents except for dicholoromethane (DCM) and tetrahydrofuran (THF), sodium borohydride ($NaBH_4$) and triethylamine were purchased from FUJIFILM Wako Pure Chemical Corporation. Tetraphenylphosphonium chloride (PPh_4Cl) and 3,5-bis(trifluoromethyl)ethynylbenzene ($RC\equiv CH$) were purchased from Tokyo Chemical Industry. DCM, THF, and Sodium hydrogen carbonate ($NaHCO_3$) were purchased from Kanto Chemicals. Chloro(2-methylphenyl)bis(triphenylphosphine) nickel (II) (Ni(o-toryl)Cl(PPh_3)$_2$) was purchased from Sigma-Aldrich. All water used was Milli-Q grade (>18 MΩ). All commercially available reagents were used as received. $Ph_3P(AuCl)$, $Me_2S(AuCl)$, $[PdAu_8(PPh_3)_8](NO_3)_2$, and $[PtAu_8(PPh_3)_8](NO_3)_2$ are synthesized according to the previous reports.[1-4]

$[PdAu_{24}(C\equiv CR)_{18}](PPh_4)_2$

The synthesis was conducted according to the previous report.[4] (Me_2S)AuCl (35.7 mg, 120 µmol) was suspended in THF (2 mL) and stirred in the dark. $RC\equiv CH$ (15.1 µL, 90 mol) and triethylamine (12.5 µL, 90 µmol) were added, resulting in a colorless solution (solution **A**) containing Au-C≡CR polymer complexes. $[PdAu_8(PPh_3)_8](NO_3)_2$ (20.3 mg, 5 µmol) was dissolved in a mixed solution of EtOH (500 µL) and THF (5 mL) in another test tube and the solution was cooled in an ice bath. Then, an ethanolic solution of $NaBH_4$ (0.10 M, 50 µL) was added to this chilled solution and after 30 s, solution **A** was added dropwise over 2–3 min. After stirring for 30 min, PPh_4Cl (3.7 mg, 10 µmol) in MeOH (1 mL) was added to the solution and the stirring was continued for 10 min. The crude mixture was poured into cold hexane (160 mL) and stirred for 1 h. The precipitate was collected by centrifugation and washed three times with cold hexane. The resulting crude product was extracted with an EtOH:toluene = 1:1 mixture (3 mL) and reprecipitated with cold hexane (50 mL). The precipitate was collected by centrifugation and extracted with Et_2O (4 mL). The supernatant was precipitated with hexane (20 mL) and dried in vacuo. The yield was 17.7 mg (36% based on the initial Pd).

$[PtAu_{24}(C\equiv CR)_{18}](PPh_4)_2$

The synthesis was conducted according to the previous report.[4] The procedure is the same with 2.1.1 except for the use of $[PtAu_8(PPh_3)_8](NO_3)_2$ (20.2 mg, 5 µmol) instead of $[PdAu_8(PPh_3)_8](NO_3)_2$. The yield was 21.9 mg (44% based on the initial Pt).

$[NiAu_{24}(C\equiv CR)_{18}](PPh_4)_2$

The synthesis was conducted according to the previous report.[5] A large test tube heated at 45 °C was charged with $Ph_3P(AuCl)$ (223.2 mg: 0.45 mmol) and Ni(o-toryl)Cl(PPh_3)$_2$ (71.9 mg: 0.1 mmol) and a magnetic stir bar. A volume of 50 mL of dry DCM was added to the tube and the yellow solution was stirred at 45 °C for 1 min. A freshly prepared ethanolic solution of $NaBH_4$ (50 mg: 1.3 mmol in 3 mL) at 0 °C was added to the hot, stirred solution at once, causing a fast color change from yellow to black. After stirring for 2 h, the solution was cooled in an ice bath and aqueous $NaHCO_3$ (1 M, 10 mL) was slowly added to the cooled solution. The aqueous phase was removed by pipet and the DCM solution was dried over $MgSO_4$. The $MgSO_4$ was filtered through folded filter paper and the filtrate was evaporated to dryness. The residue was extracted by DCM (5 mL) and the insoluble material was removed by centrifugation. The supernatant was added to toluene (20 mL) and diisopropyl ether (12.5 mL). The mixture was centrifuged to collect the reddish brown solid and the supernatant was added hexane (15 mL) to collect the solid. Both solids were put together and used as crude $[HNiAu_9(PPh_3)_8Cl]Cl$ in the next step. (Me_2S)AuCl (70.1 mg, 240 µmol) was suspended in THF (2 mL) and stirred in the dark. RC≡CH (30.2 µL, 180 mol) and triethylamine (25 µL, 180 µmol) were added, resulting in a colorless solution (solution **A**) containing Au–C≡CR polymer complexes. Crude [HNiAu$_9$(PPh$_3$)$_8$Cl]Cl (39.9 mg) was dissolved in a mixed solution of DCM (2.5 mL) and THF (5 mL) in another test tube and the solution was cooled in an ice bath. Solution **A** was added to the solution dropwise over 2–3 min. After stirring for 20 min, PPh$_4$Cl (7.4 mg, 20 µmol) in MeOH (1 mL) was added to the solution and the stirring was continued for 5 min. The crude mixture was poured into cold hexane (200 mL) and stirred for 45 min. The precipitate was collected by centrifugation and washed three times with cold hexane. The resulting crude product was extracted with an EtOH:toluene = 1:1 mixture (6 mL) and reprecipitated with cold hexane (40 mL). The precipitate was collected by centrifugation and extracted with Et$_2$O (4 mL). The supernatant was precipitated with hexane (25 mL) and dried in vacuo. The yield was 9.0 mg.

Theoretical Methods

Trajectory calculations in ImoS

Collision cross sections (CCSs) were calculated with the trajectory method as implemented in IMoS 1.09.[6, 7] The atomic coordinates of the geometry optimized DFT structures and their corresponding NBO partial charges[8] were used as input data. In IMoS, the interaction of the ions with the collision gas N_2 is modeled with a Lennard-Jones (LJ)-type interaction and an additional ion-induced dipole potential. Due to the anisotropy of N_2, the ion–quadrupole interaction (qpol) was taken into account explicitly. Therefore, the total interaction potential is given by

$$U(x,y,z) = \sum_{l=1}^{\text{atoms}} 4\varepsilon_l \left(\left(\frac{\sigma_l}{R_l} \right)^{12} - \left(\frac{\sigma_l}{R_l} \right)^{6} \right) - \left(\frac{\alpha}{2} \sum_{i=1}^{3} \left(\sum_{l=1}^{\text{atoms}} \frac{X_{il} q_l}{R_l^3} \right)^2 \right) - \sum_{i=1}^{3} \left(\sum_{l=1}^{\text{atoms}} \frac{q_l q_i}{R_{il}} \right)$$

where ε and σ are the atom specific LJ parameters, R_l is the distance between the atom *l* and N_2 and X_{il} are its Cartesian components, α is the polarizability volume of N_2 (1.74 Å^3), q_l are the atomic partial charges of the cluster, and q_i are the three partial charges on N_2 (assumed to be -0.4825 on each nitrogen and +0.965 at the center) to reproduce the bulk quadrupole moment of N_2. As S and Au is not parametrized in IMoS, we used the unchanged default values. Based on the ion-nitrogen interaction potential, the scattering angle (χ) was calculated by a series of $3 \cdot 10^6$ trajectory calculations and the momentum transfer cross section ($^{\text{TM}}\text{CCS}_{\text{N2}}$) was obtained by numerical integration of χ with IMoS. For the structures of the precursor ions the series was repeated at least 10 times ($3 \cdot 10^7$ trajectory calculations) to increase accuracy and to obtain statistical errors.

Experimental Methods

Brief description of the IMS/MS sequences used

For a detailed description of the instrument we refer to the publication of Giles et al.[9] Here only the components relevant to the experiments presented are decribed briefly. Like in the older Waters Synapt G2 instrument, the Select Series Cyclic IMS comprises a quadrupole that can be operated as a mass filter or as an ion guide, followed by an ion mobility cell and a time-of-flight mass spectrometer (MS-IMS-MS). The major difference to Synapt G2 is the cylic IMS cell (cIM) that is orthogonal to the regular ion path. By adjusting the voltages and timings of the T-wave-array the respective ion packet can be transferred into the cIM, or out of it, or simply passed through and the number of cycles in cIM can be adjusted. If the IMS functionality is not used („TOF mode"), the T-wave array is set permanently in the „forward" direction, i.e. the ions leaving the trap pass pre and post store and are directly transferred to the reflectron time of flight mass spectrometer that can be operated either in „V-mode" or „W-mode" with a mass resolution exceeding 100000. In „IMS mode" the T-wave array is operated „sideways" for a short time, i.e. the ion packet is injected from the pre store into the Cyclic IMS. The timing of the T-wave array sets the number of cycles: as long as it stays in the „sideways mode", the ions keep cycling, switching it to the „forward" direction transfers the ions toward the time-of-flight mass spectrometer.

For the IMS experiments of the parent ions described in the main text (see figure 2) the quadrupole is operated as ion guide and the three $[MAu_{24}(C{\equiv}CR)_{18}]^{2-}$ (M=Ni, Pd, Pt) dianions are injected simultaneously in order to get their CCS differences as accurately as possible. Note however, that the IMS determination is still mass selective because for each time-bin of the arrival time distribution a complete high-resolution time-of-flight mass spectrum is recorded.

For the high-resolution IM separation of three doped gold cluster $[MAu_{24}(C{\equiv}CR)_{18}]^{2-}$ (M=Ni, Pd, Pt) we performed up to 50 cycles corresponding to a cycle time of 1100 ms (see figure 2). The travelling wave parameters were TW-static height 22V and velocity 375 m/s, which are the default values for the instrument.

In the CID experiments (see figure S3-S5) the quadrupole mass filter is set to the respective parent mass. The fragmentation occurs in the trap downstream the quadrupole by collisions with nitrogen. The collision energy is set in the range of 10 to 200 V, depending on the desired fragmentation degree. The cIM is bypassed in this mode (TOF mode) and the fragment ions are analyzed in the time-of-flight mass spectrometer (V-mode).

In the CID+IMS experiments of the fragments (see figure 4), the respective parent ion is selected in the quadrupole are injected with variable energy into the trap. All emerging fragments are then simultaneously put into the cIM for one (see figure 4) or multiple (see figure 6) cycles - and then analysed mass selectively).

IMS^2 experiments were performed by switching the T-wave array „backwards", thereby putting the ion packet (selected by the timing of the T-wave array switching) back into the pre store. In a subsequent step the ions stored in the pre store can then be reinjected into the cIM and the injection energy can be varied in order to induce isomerization and/or further fragmentation.

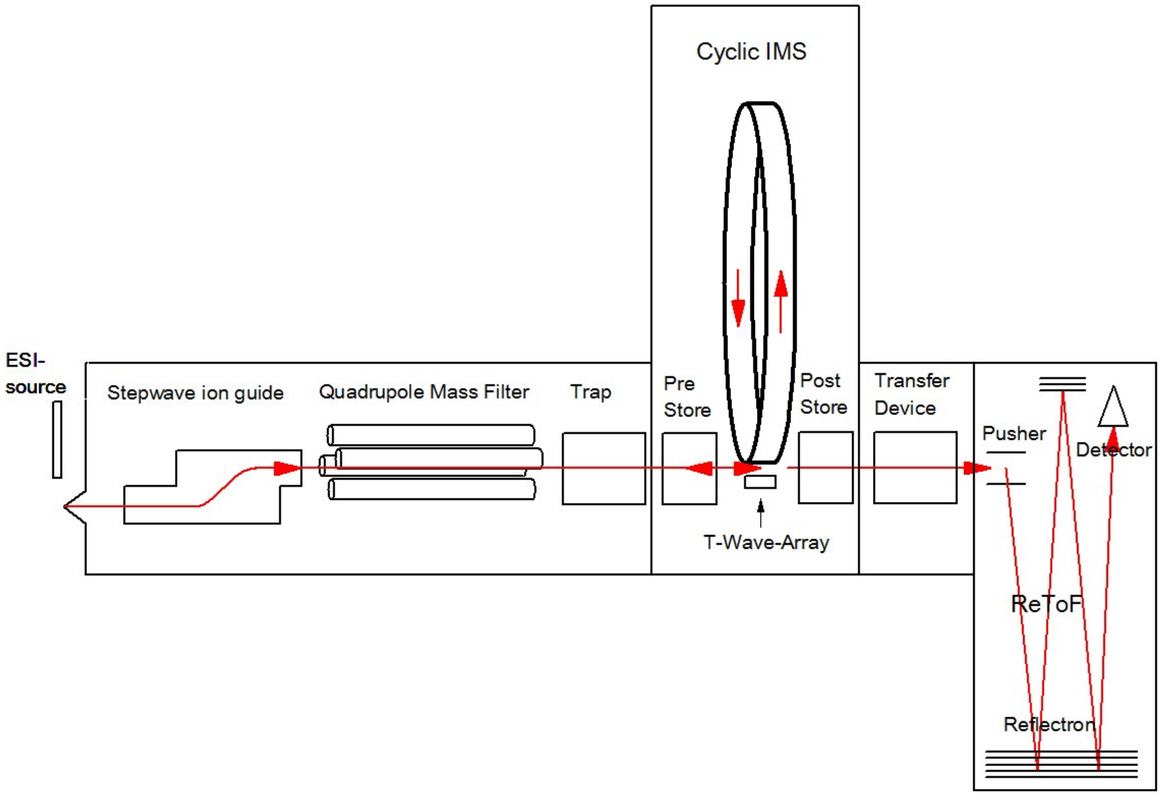

Scheme S1: Instrument schematic. See text (and ref. 4) for details.

Calibration procedure

The collision cross section (CCS) of an ion and its reduced mobility (K_0) are related by the Mason-Schamp equation,[10] with T the temperature, N_0 the number density of the buffer gas, k_B Boltzmann´s constant, $z \cdot e$ the ion charge and μ the reduced mass of the drifting ion and the buffer gas molecules (N_2)

$$CCS = \frac{3}{16}\sqrt{\frac{2\pi}{\mu \cdot k_B \cdot T}} \cdot \frac{ze}{N_0} \cdot \frac{1}{K_0}$$

Often this equation is rearranged by putting the ion specific reduced mass and charge to the left and introducing a mass and charge corrected collision cross section, CCS', which is inversely proportional to the reduced mobility.

$$CCS^{'} = \frac{CCS\sqrt{\mu}}{z} = \frac{3}{16}\sqrt{\frac{2\pi}{k_B \cdot T}} \cdot \frac{e}{N_0} \cdot \frac{1}{K_0}$$

In drift tube instruments the drift time t_d of an ion is inversely proportional to its mobility and therefore CCS' depends linearly on the measured arrival time $t=t_d+t_0$ (with some offset t_0 due to the time the ion spend outside of the drift cell prior to detection). In travelling wave instruments the relation between drift time and CCS' is not linear. It is often described by the equation[11]

$$CCS^{'} = A \cdot t_d{}^m = A \cdot (t - t_0)^m$$

Furthermore, unlike in drift tube instruments, where mobilities can be determined by first principles (by knowing pressure, temperature and electric field), travelling wave instruments need calibration. We use Agilent tunemix since it spans a wide mobility and mass range and its CCS have been determined in various labs to a high precision[12]. The workflow for a 1-cycle experiment is a follows: First, we measure the arrival time distributions of the calibrant ions and determine the peak positions by a gaussian fit. Next, we plot these times against the CCS' values based on the tabulated collision cross sections. [12] As can be seen from figure S1a for a typical 1-cycle experiment the three parameter fit (A, m, t_0) has a correlation coefficient of >0.999, i.e. the calibration data set is internally highly consistent. Furthermore, m turns out to be very close to 0.5. If we fix m to 0.5, i.e. use a square-root-law, the quality of the fit is essentially unchanged, see figure S1b. We tested this for a wide range of travelling wave parameters, in all cases a two-parameter (A,t_0) fit according to the square-root-law is essentially as good as the three-parameter-fit. For the sake of simplicity, we use the square-root-fit. The key feature of the Waters Select Series Cyclic instrument is the possibility to arbitrarily increase the drift length by increasing the number of cycles. The calibration workflow for a n-cycle experiment is similar, with the exception that the separation time for each of the calibrant and analyte ions has to be adjusted so that all ions undergo exactly the same number of cycles. Then, the same square-root-fit function can be used with similar fit quality.

A more flexible procedure is based on the time-per-cycle, by taking the difference of two arrival-time measurements at n and n+1 cycles. This procedure has the advantage that it eliminates the time the ions spend outside the cIM and therefore can be used for more complicated IMS^n experiments where the start trigger changes between analyte and calibrant and an n-cycle-arrival time fit cannot be used. Again, the square-root-law turns out to be an adequate fit function.

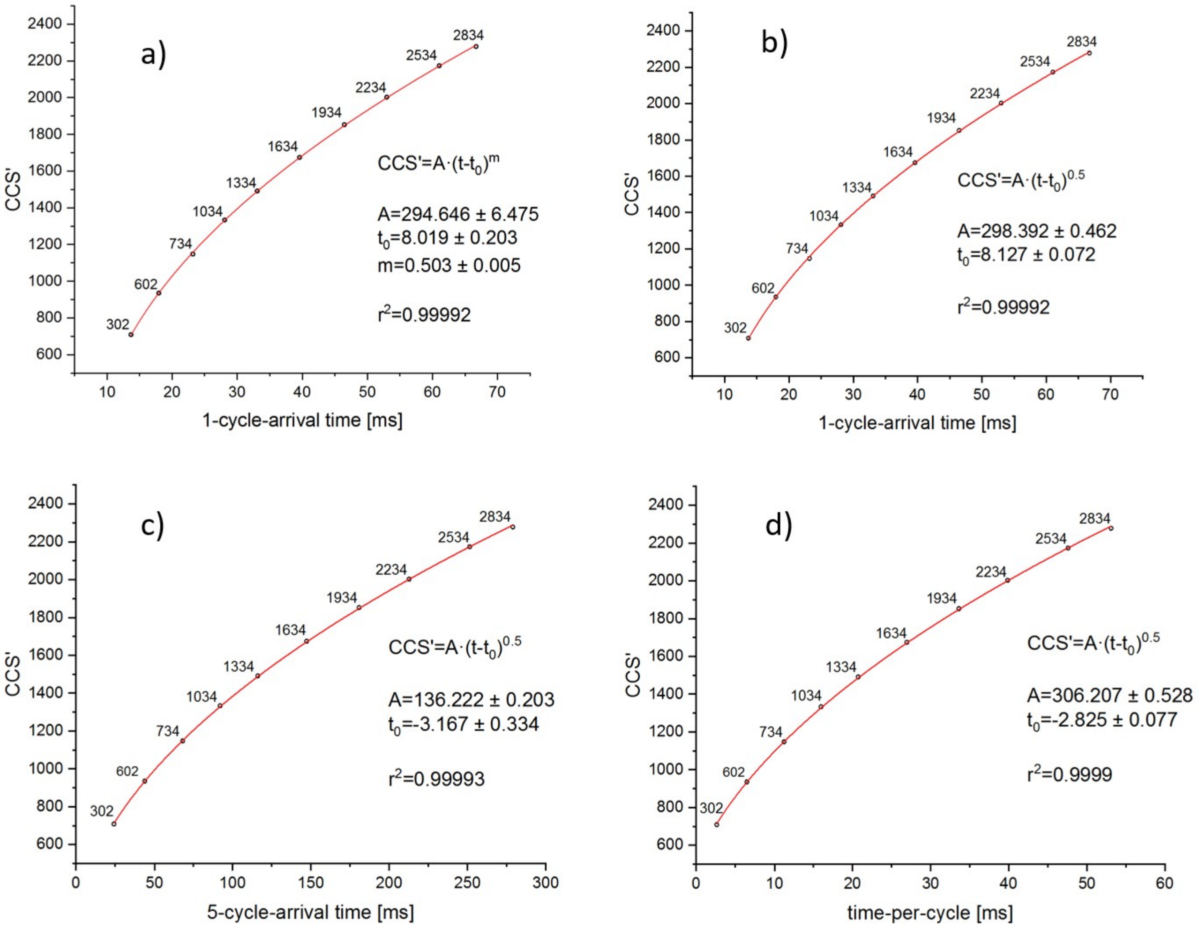

Figure S1. Calibration function. We use Agilent tunemix with the tabulated CCS-values of Stow et al. throughout. a) fit based on 1-cycle-arrival times using a three parameter fit (power law with time offset). The quality of fit is very high as can be seen by the squared correlation coefficient. b) a two parameter-fit based on a square root law with time off–et - the quality of fit is basically unchanged. c) and d) same fitting procedure based on arrival time after 5 cycles and time-per-cycle. The parameters A and t_0 depend on the instrument settings (travelling height and speed, temperature, buffer gas pressure) and are determined daily. The parameters shown are typical values for default TW-height and -speed (22 V and 375 m/s).

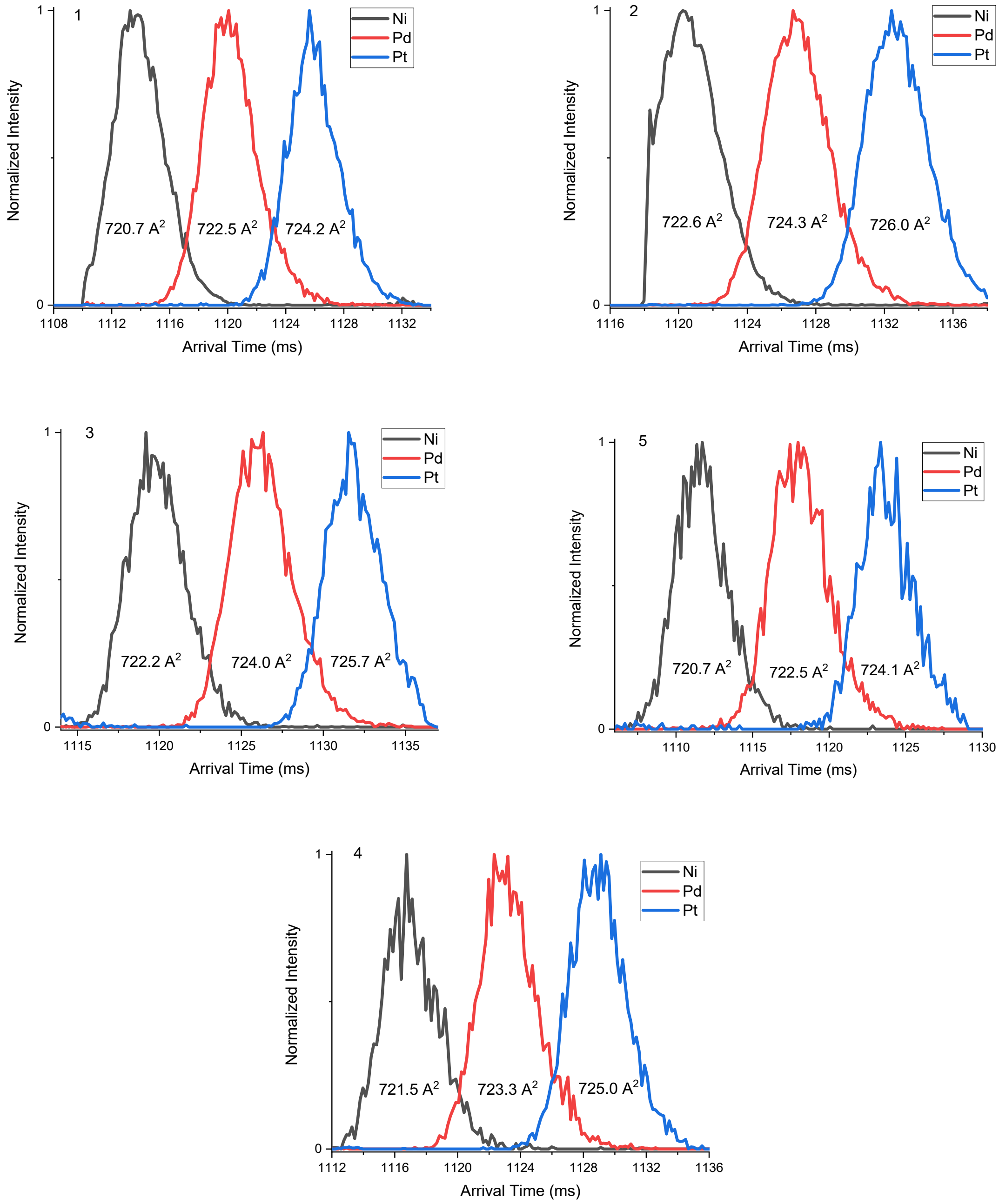

Figure S2. Comparison of arrival time distributions for all three parent dianions at the lowest possible internal excitation levels (50 separation cycles; 50V) – see also figure 2 in main text. All M show only one, symmetric ATD, i.e. the excitation energy is below threshold for NiAu24 isomerization. Shown are five different measurements on five different MAu24 mixtures to highlight the precision of $\Delta^{tw}CCS_{N2}$ determinations.

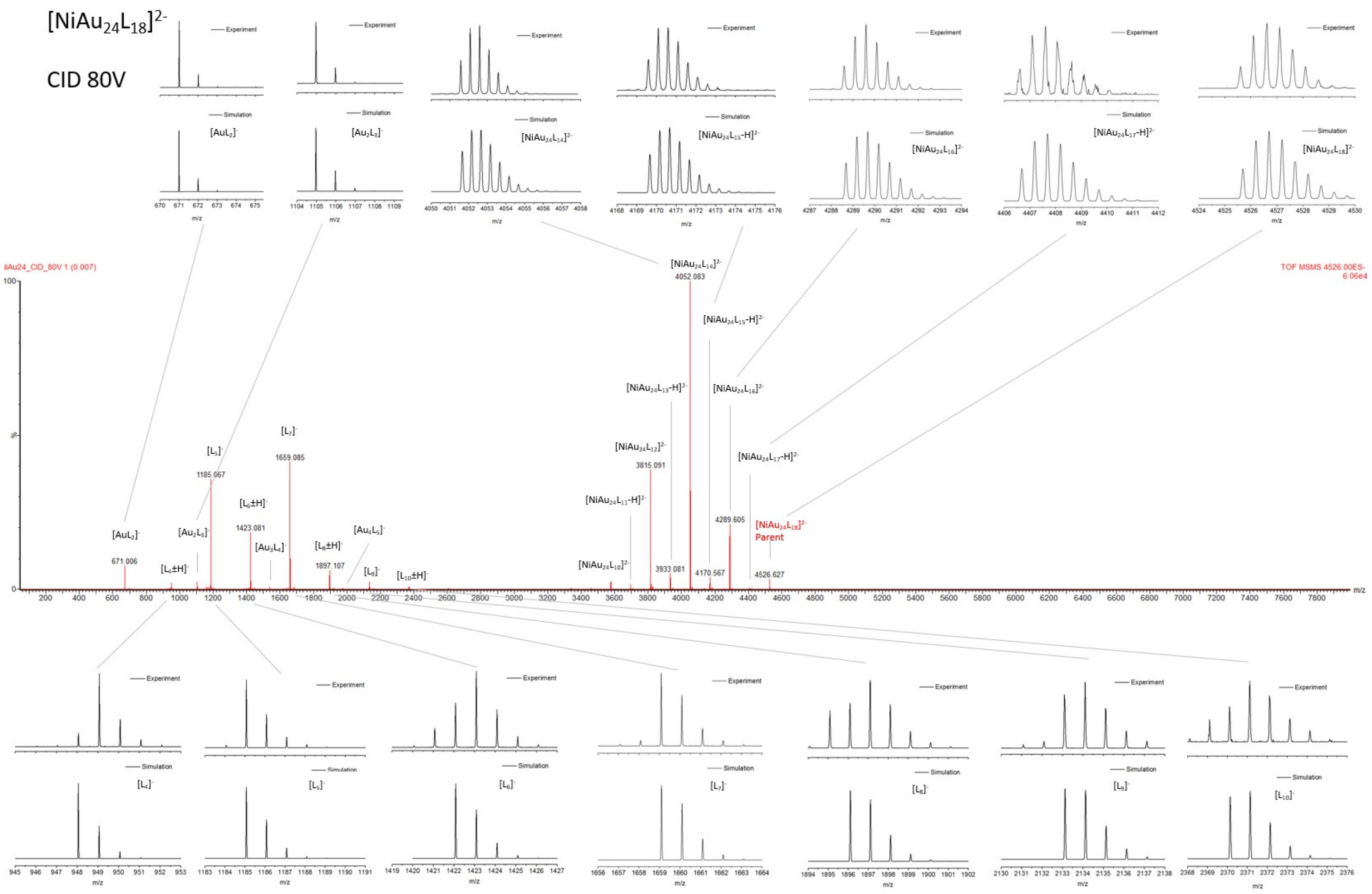

Fig. S3a. Collision induced dissociation of [NiAu$_{24}$L$_{18}$]$^{2-}$ at 80 V collision voltage, mass spectrum and assignment of fragment ions (L refers to the alkyne ligand C≡CR, with R =3,5-(CF$_3$)$_2$C$_6$H$_3$, see main text). The difference between the experimental and simulated mass spectra of [L$_n$]$^-$ (especially for the even numbered fragment ions) is due to intramolecular hydrogen transfer, i.e. the experimentally observed fragment mass spectra correspond to a mixture of [L$_n$]$^-$, [L$_n$+H]$^-$ and [L$_n$-H]$^-$.

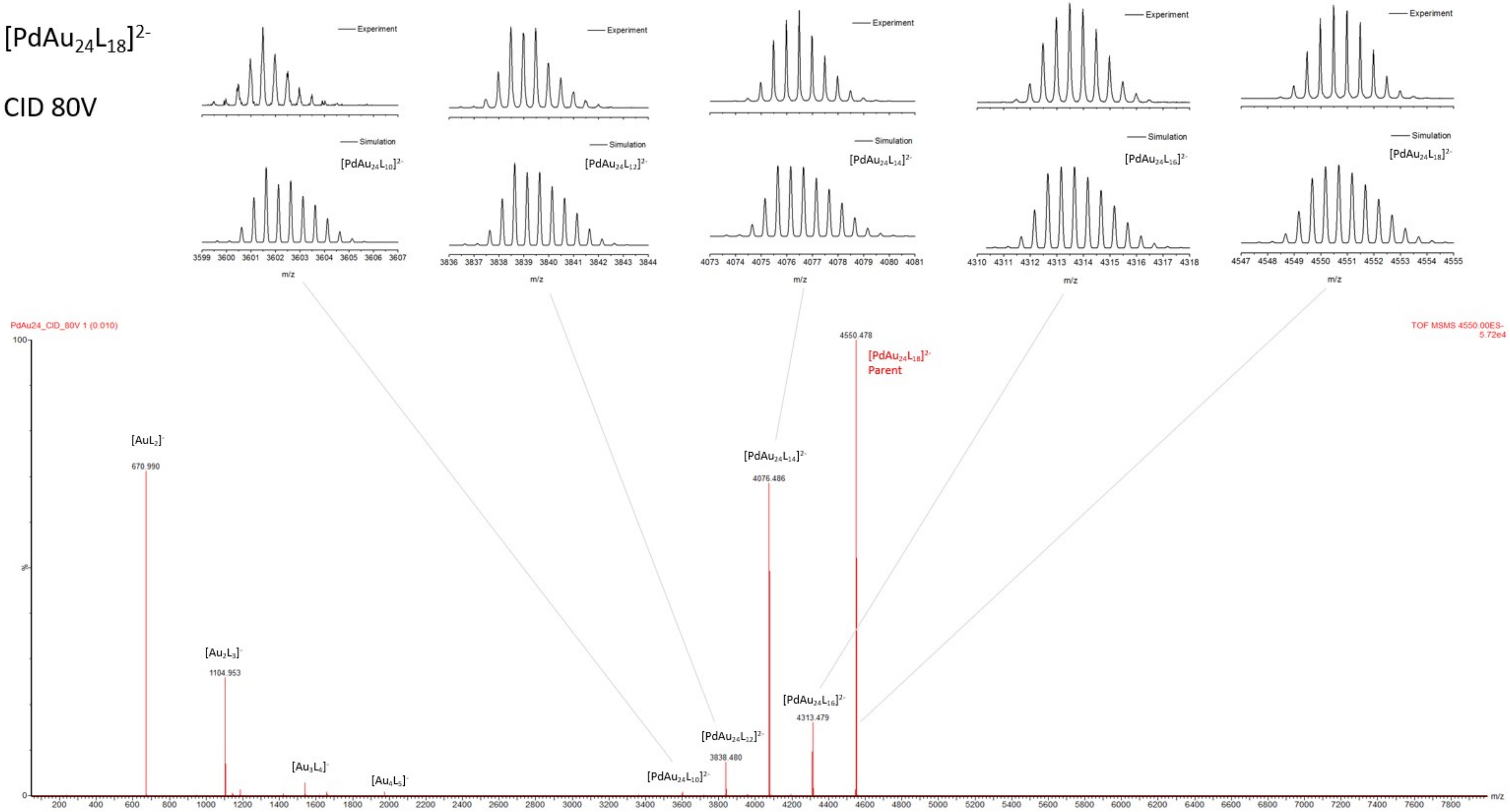

Fig. S3b. Collision induced dissociation of $[PdAu_{24}L_{18}]^{2-}$ at 80 V collision voltage, mass spectrum and assignment of fragment ions.

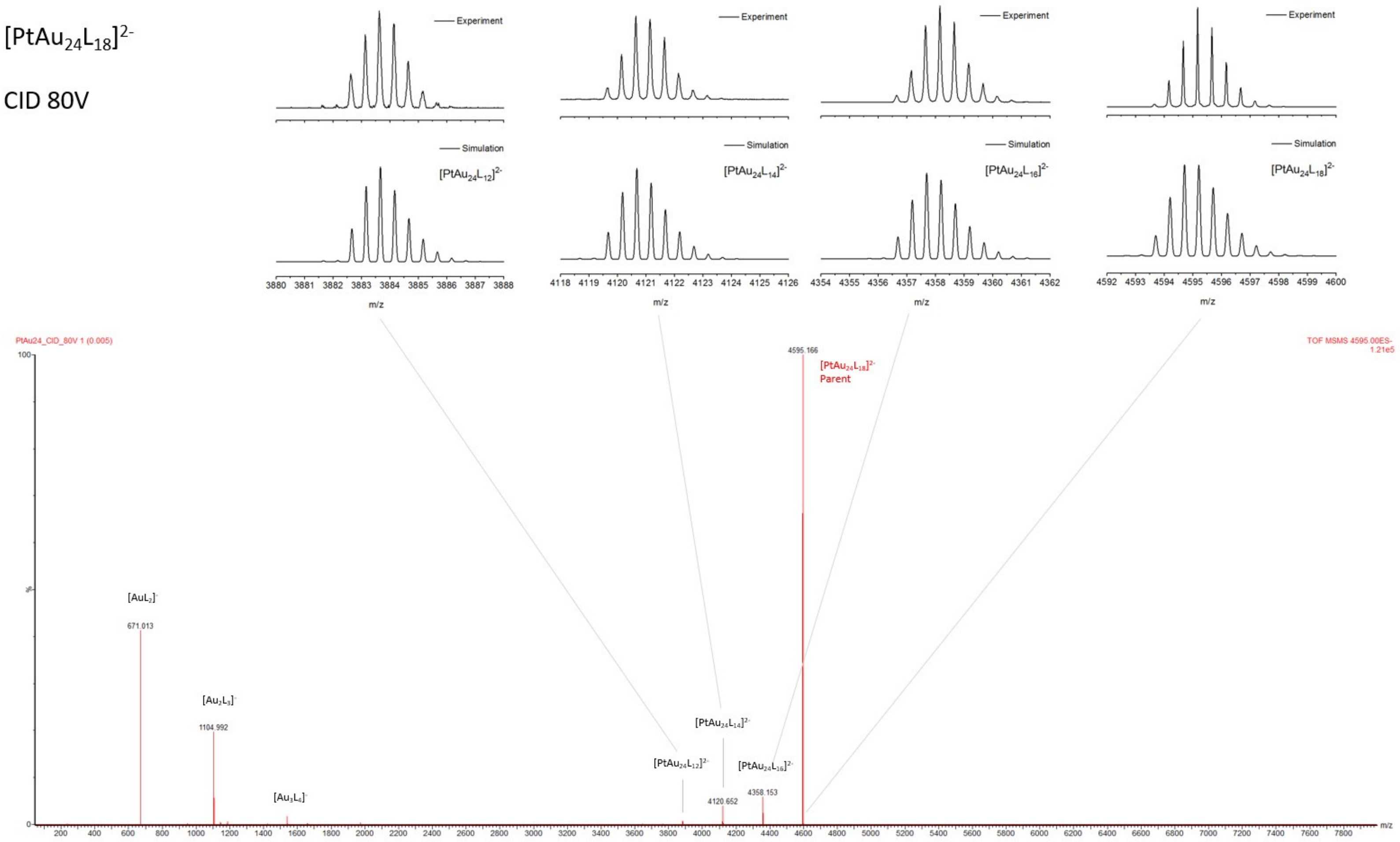

Fig. S3c. Collision induced dissociation of $[PtAu_{24}L_{18}]^{2-}$ at 80 V collision voltage, mass spectrum and assignment of fragment ions.

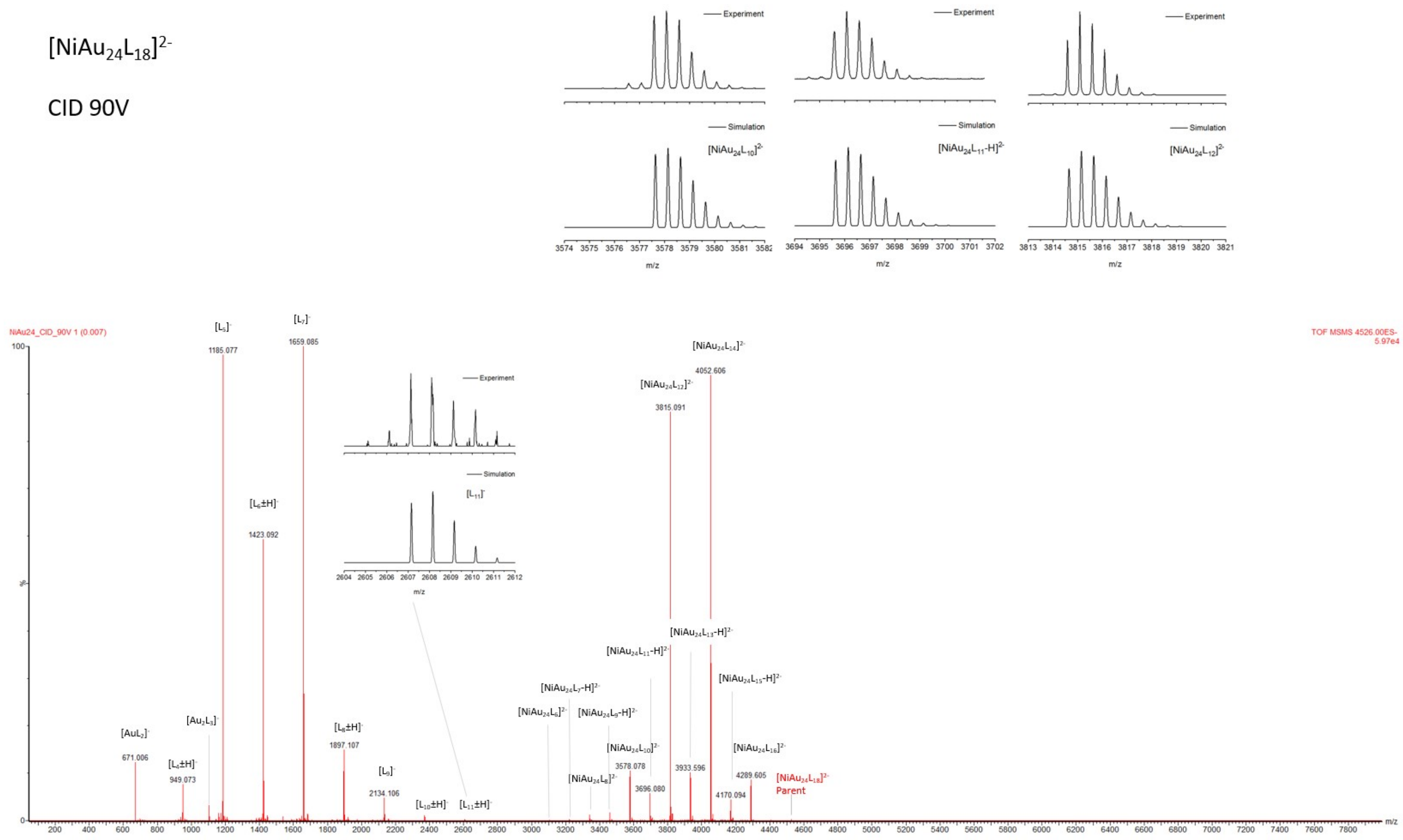

Fig. S4a. Collision induced dissociation of $[NiAu_{24}L_{18}]^{2-}$ at 90 V collision voltage, mass spectrum and assignment of fragment ions (L refers to the alkyne ligand C≡CR, with R =3,5-$(CF_3)_2C_6H_3$, see main text)

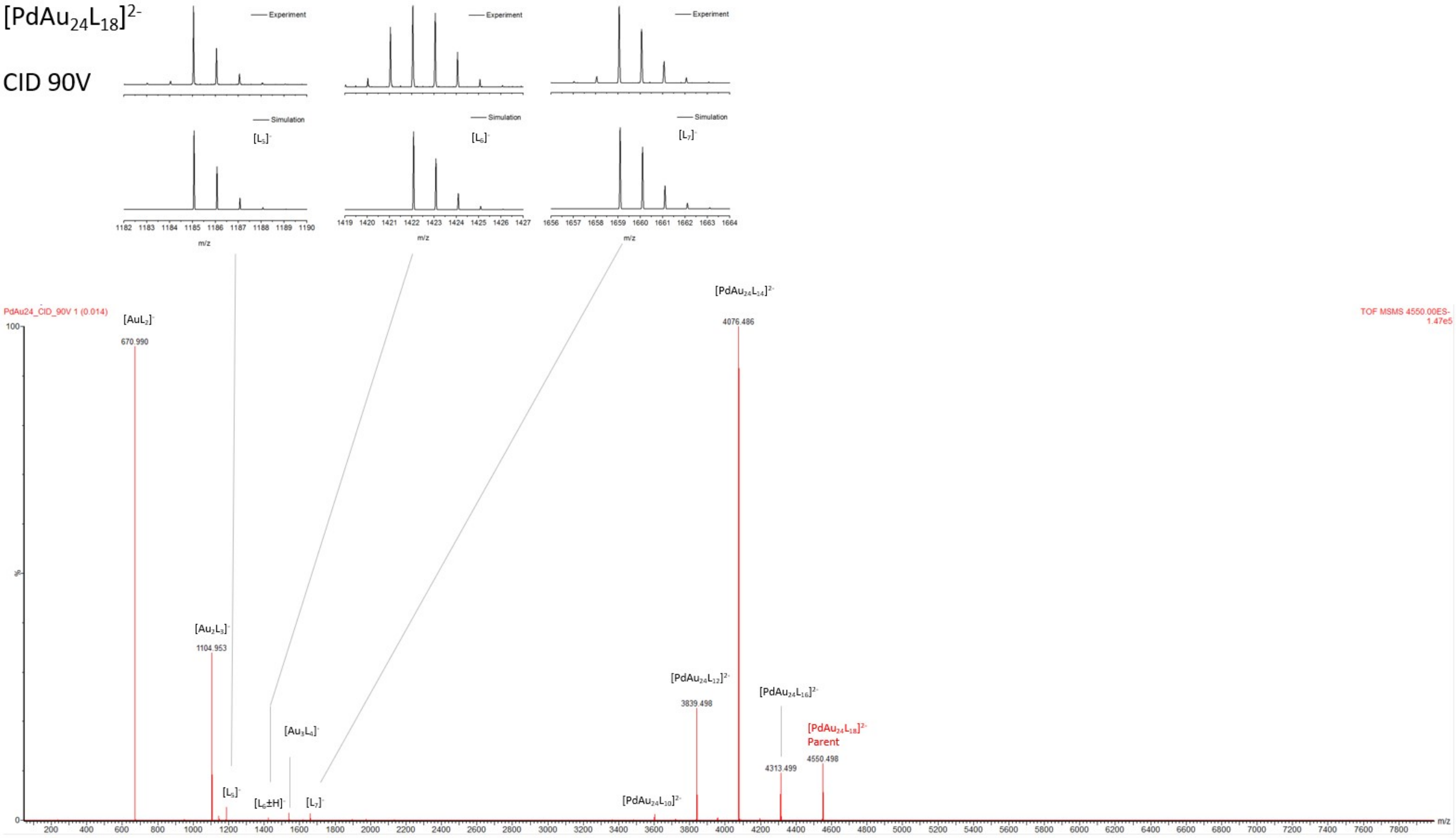

Fig. S4b. Collision induced dissociation of [PdAu$_{24}$L$_{18}$]$^{2-}$ at 90 V collision voltage, mass spectrum and assignment of fragment ions.

$[PtAu_{24}L_{18}]^{2-}$

CID 90V

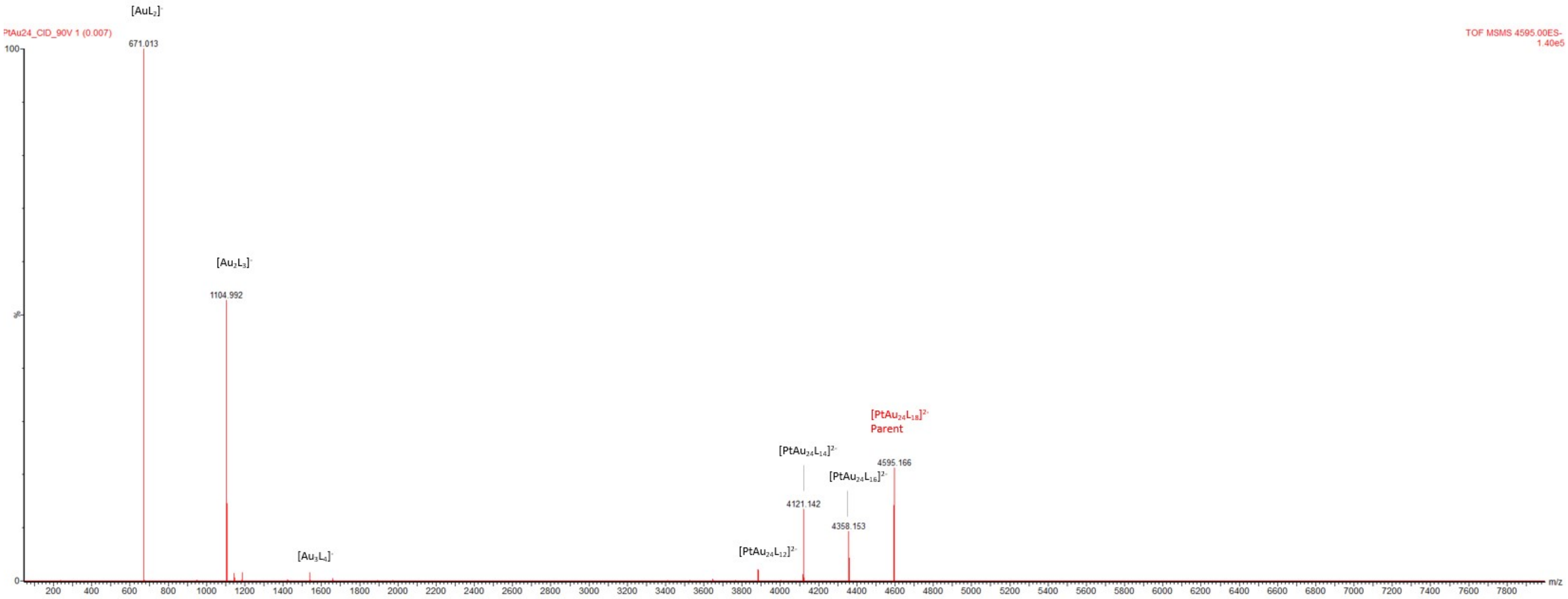

Fig. S4c. Collision induced dissociation of $[PtAu_{24}L_{18}]^{2-}$ at 90 V collision voltage, mass spectrum and assignment of fragment ions.

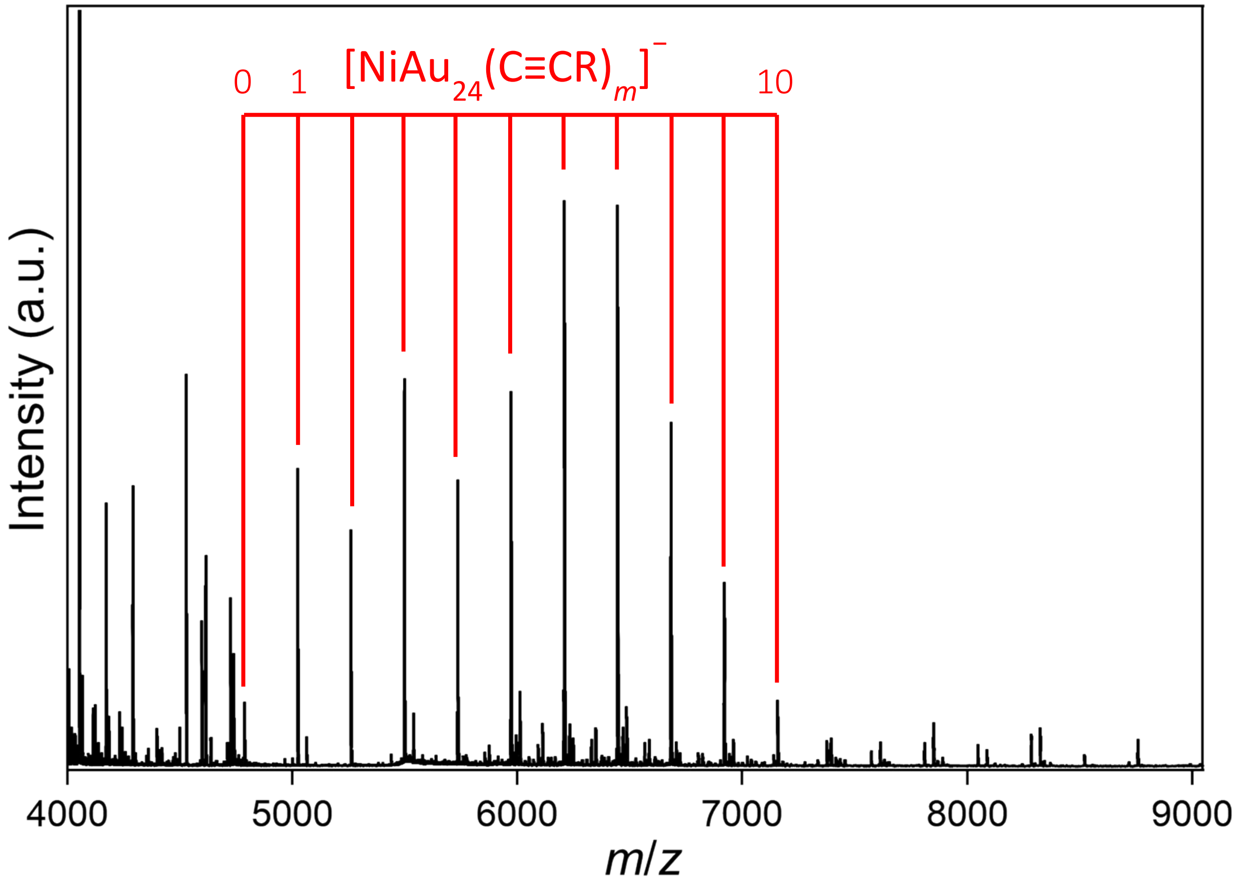

Fig. S5. Collision induced dissociation of $[NiAu_{24}L_{18}]^{2-}$ at nominally 200 eV collision energy as studied with a Bruker compact ESI-MS. The high m/z range spectrum documents the formation of $[NiAu_{24}L_m]^{1-}$ fragments, m= 0–10, under conditions in which L_n^- polymers can also be observed (reaction 2 main text).

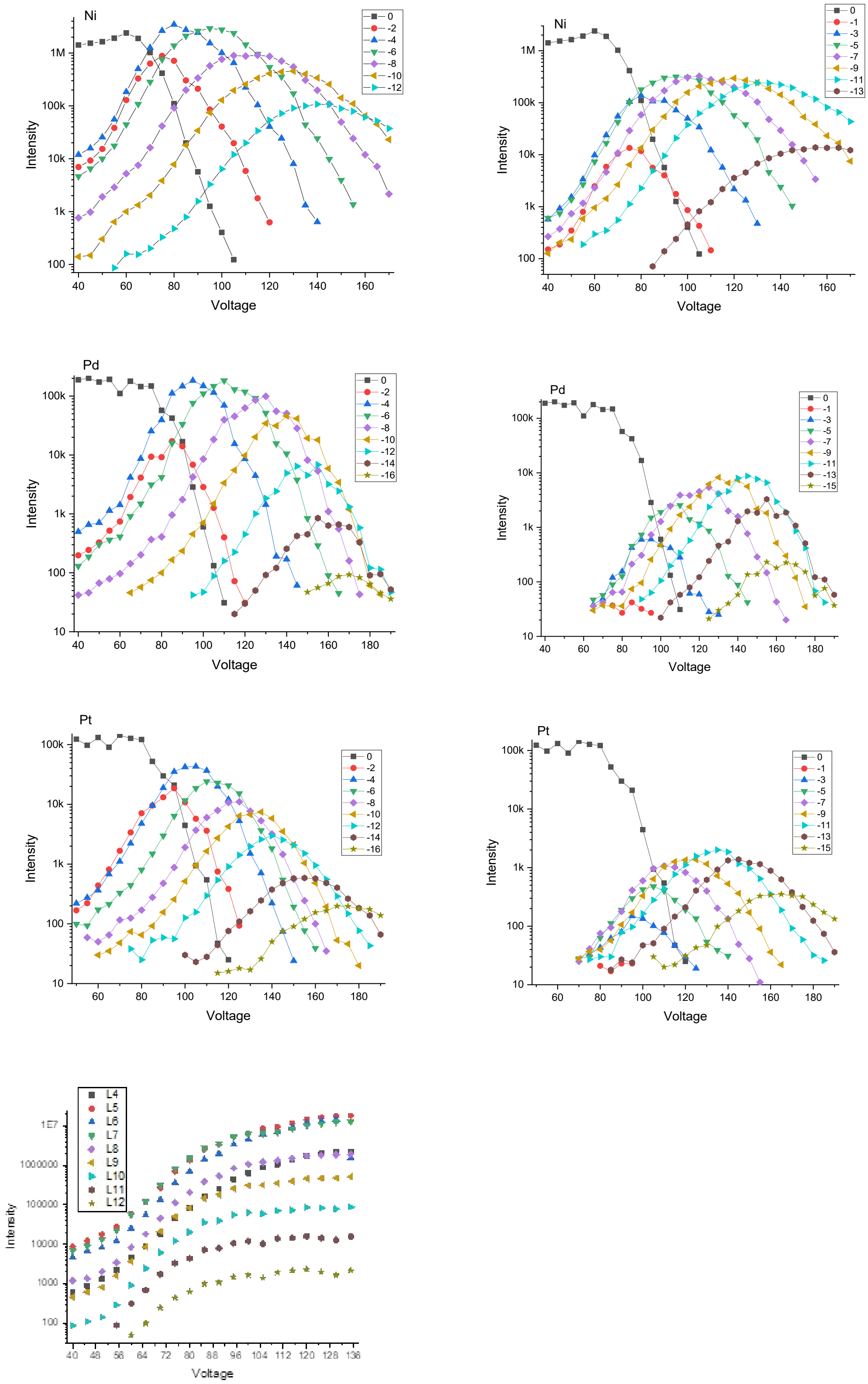

Figure S6: Top six plots show breakdown curves and corresponding fragment yields versus collision voltage for all three $[MAu_{24}L_{18}]^{2-}$ as indicated (left frames: even numbers of ligands; right frames: odd numbers). The bottom frame shows the appearance thresholds for L_x^- oligomers observed for $[NiAu_{24}L_{18}]^{2-}$ CID.

M = Pt (*n* = 2–8; *n* = 10 in main text):

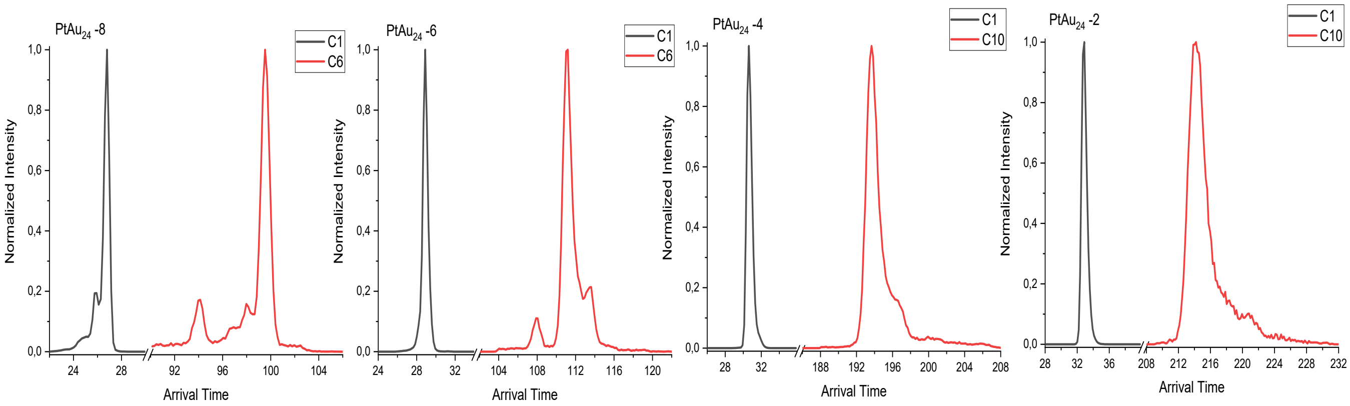

M = Pd (n = 2–8)

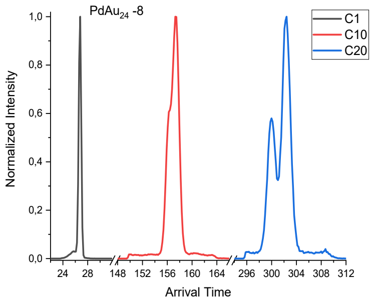
PdAu$_{24}$ -8
C1
C10
C20
Normalized Intensity
1,0
0,8
0,6
0,4
0,2
0,0
24
28
148
152
156
160
164
296
300
304
308
312
Arrival Time

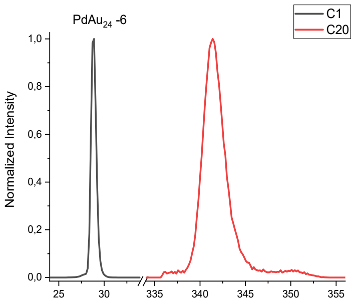
PdAu$_{24}$ -6
C1
C20
Normalized Intensity
1,0
0,8
0,6
0,4
0,2
0,0
25
30
335
340
345
350
355
Arrival Time

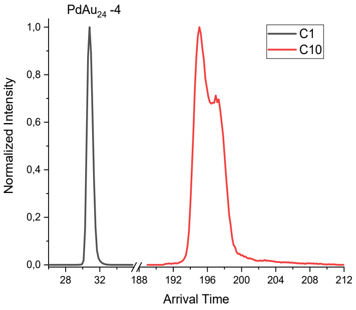
PdAu$_{24}$ -4
C1
C10
Normalized Intensity
1,0
0,8
0,6
0,4
0,2
0,0
28
32
188
192
196
200
204
208
212
Arrival Time

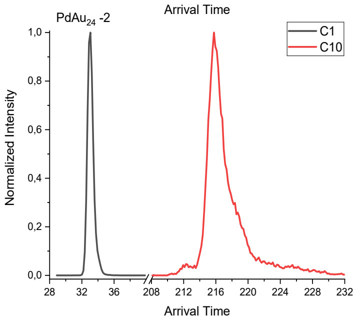
PdAu$_{24}$ -2
C1
C10
Normalized Intensity
1,0
0,8
0,6
0,4
0,2
0,0
28
32
36
208
212
216
220
224
228
232
Arrival Time

M = Ni (*n* = 2–8)

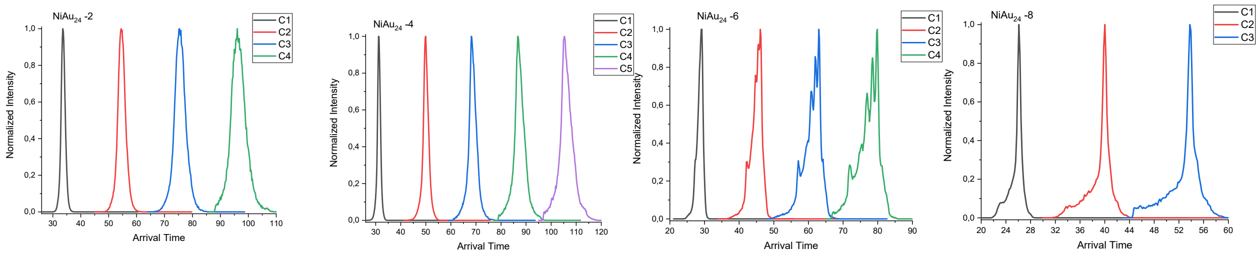

Figure S7: Mobilograms of selected $[MAu_{24}L_{18-n}]^{2-}$ fragments generated upon CID of $[MAu_{24}L_{18}]^{2-}$ versus *n* the number of ligands lost. ATD are shown for different numbers of separation cycles as indicated. Note, that the isomer space is strongly dependent on *n* and M.

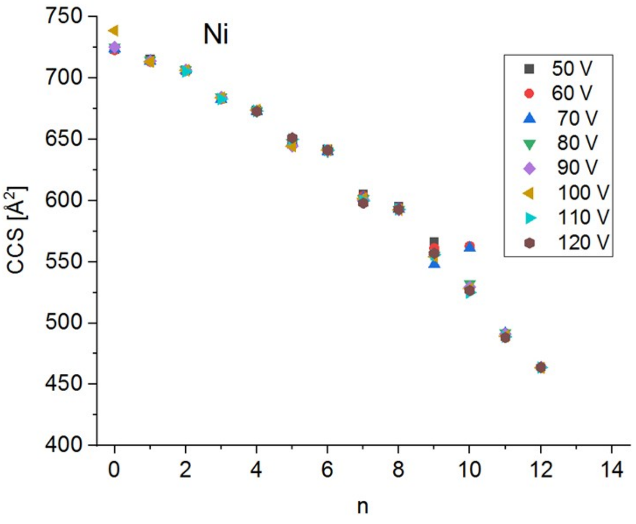

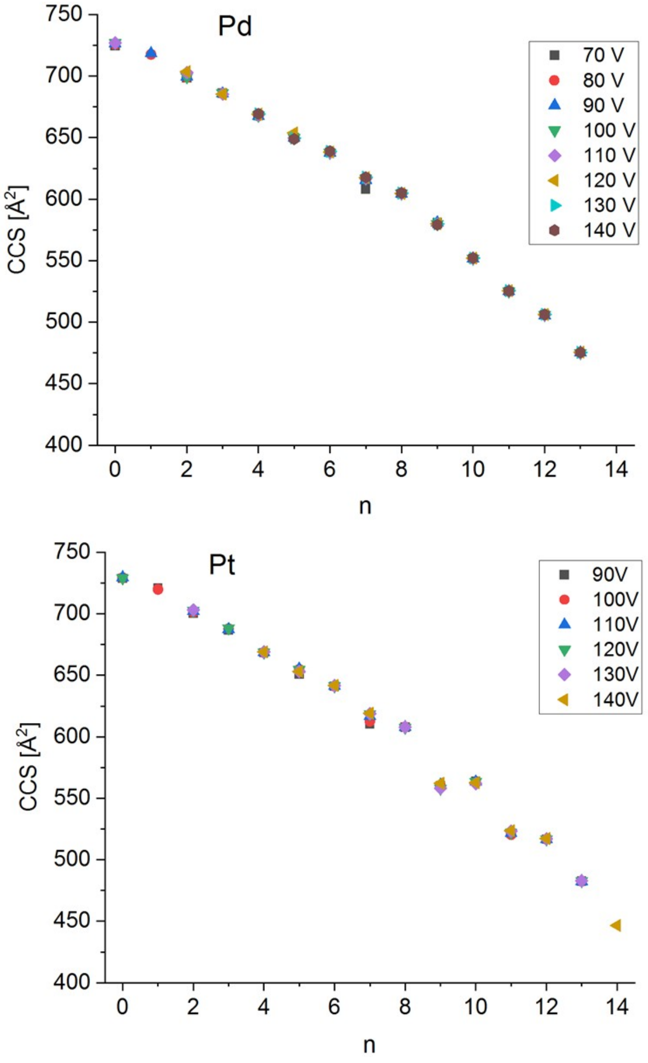

Figure S8: Average $^{tw}CCS_{N2}$ of fragments $[MAu_{24}L_{18-n}]^{2-}$ versus *n* the number of ligands lost upon CID of the parent $[MAu_{24}L_{18}]^{2-}$ (on the basis of single cycle separations). Note that while the overall intensities of specific fragments *n* change significantly with collision voltage, $^{tw}CCS_{N2}$ values remain roughly constant.

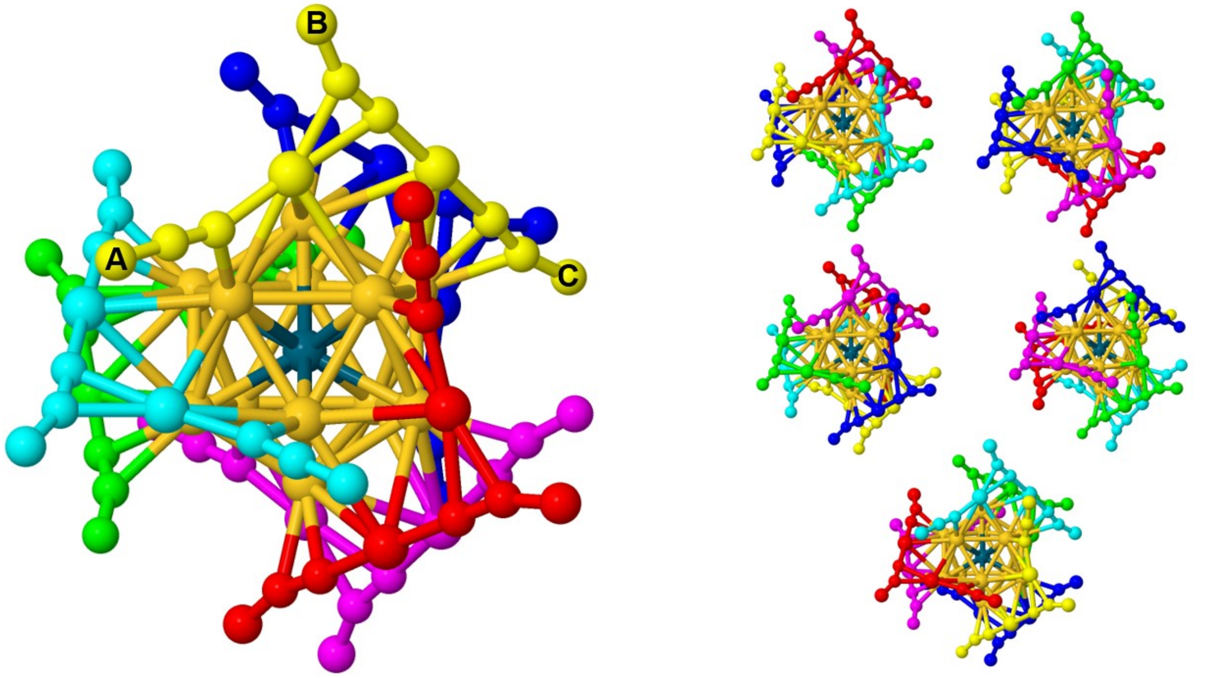

Figure S9: DFT structure of $[PdAu_{24}L_{18-n}]^{2-}$ with each of the six staples colored differently. For clarity we show only the three terminal carbon atoms of a given ligand (Φ**C-C≡C**; see also scheme 1 main text). To generate different fragment isomers, we removed ligand types A and B from the staples to form even *n* fragments and one additional randomly selected type A ligand for odd *n* fragments. The parent dianion has D3 symmetry, i.e. all six staples are equivalent as seen in the smaller images on the right which shows views of the molecule along the other five equivalent symmetry axes.

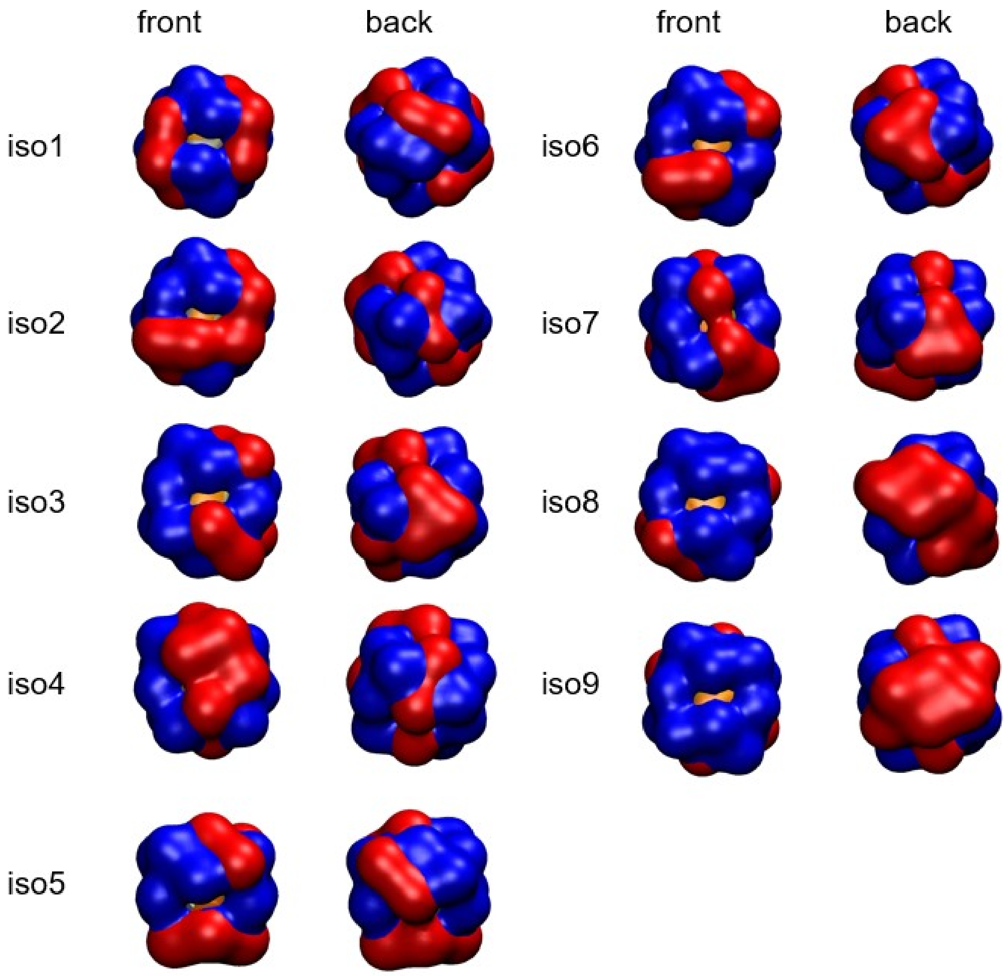

Figure S10: Schematic representations of defected model structures for the $[PdAu_{24}(C{\equiv}CR)_8]^{2-}$ fragment from Table S2 (front and back views). The red positions refer to terminal C-atoms of each remaining (C≡CR) ligand - neglecting the rest of the ligand in the representation. Blue positions refer to defect sites (again terminal C-atom positions) from which (C≡CR) ligands have been removed.

Table S1. ${}^{\mathrm{tw}}\mathrm{CCS}_{\mathrm{N2}}$ of fragments $[\mathrm{MAu}_{24}\mathrm{L}_{18-n}]^{2-}$ versus *n* the number of ligands lost (on the basis of single cycle separations). See also figure S8.

n	**Ni CCS / Å²**	**Pd CCS / Å²**	**Pt CCS / Å²**
0	721.5	723.3	724.9
1	714.2	718.0	720.4
2	706.4	700.4	701.4
3	683.6	685.7	687.5
4	673.4	668.4	668.6
5	647.4	650.2	653.6
6	641.0	638.1	641.3
7	601.6	616.9	618.3
8	593.2	604.6	607.7
9	554.5	580.0	575.3
10	528.3	551.9	562.9
11	490.4	525.3	522.1
12	463.7	506.0	516.8
13		475.3	482.7
14			446.5

Table S2: Structural models for $[PdAu_{24}(C{\equiv}CR)_8]^{2-}$ isomers and resulting ${}^{theo}CCS_{N2}$ values (see main text and figure S10 for details) ordered according to the number of ligands remaining on each of the six Au_2 staples (with colours referring to figure S9). These possible fragment structures (among many more combinatorial possibilities) were generated by starting from the relaxed $[PdAu_{24}(C{\equiv}CR)_{18}]^{2-}$ structure and removing 3, 2, 1 or 0 ligands from each of the 6 staples (see Fig S9 for the color code) to yield different isomers (without allowing for structural relaxation). Isomers 1 – 7 are isomers for which ligands were removed in a quasi-statistical way while isomers 8 and 9 are isomers where defect sites are distributed unequally in a spatially correlated fashion. Structures of bold isomers are shown explicitly in figure 6. Column labelled with "single ligands" refers to the number of single ligands (radical formation) that needs to be removed to generate the corresponding structure.

Staple	blue	red	green	magenta	cyan	yellow	single ligands	${}^{theo}CCS_{N2}$ / Å^2
Isomer 1	**3**	**3**	**2**	**0**	**0**	**0**	**4**	**606.6**
Isomer 2	3	2	1	1	1	0	2	576.2
Isomer 3	3	2	2	1	0	0	4	592.6
Isomer 4	**3**	**1**	**1**	**1**	**1**	**1**	**0**	**553.4**
Isomer 5	2	2	2	2	0	0	6	589.3
Isomer 6	2	2	2	1	1	0	4	576.6
Isomer 7	**2**	**2**	**1**	**1**	**1**	**1**	**2**	**555.8**
Isomer 8	3	0	0	2	0	3	4	551.3
Isomer 9	**2**	**1**	**1**	**1**	**1**	**2**	**2**	**496.5**

References

1. Gregory, B. J.; Ingold, C. K., Mechanism of Electrophilic Substitution at a Saturated Carbon Atom . Part XI. Bimolecular and Unimolecular Substitution of Mercury for Gold in Alkylgold Complexes. *Journal of the Chemical Society B-Physical Organic* **1969,** (3), 276-&.
2. Brandys, M. C.; Jennings, M. C.; Puddephatt, R. J., Luminescent gold(I) macrocycles with diphosphine and 4,4′-bipyridyl ligands. *J. Chem. Soc.-Dalton Trans.* **2000,** (24), 4601-4606.
3. Takano, S.; Hirai, H.; Muramatsu, S.; Tsukuda, T., Hydride-Mediated Controlled Growth of a Bimetallic $(Pd@Au_8)^{2+}$ Superatom to a Hydride-Doped $(HPd@Au_{10})^{3+}$ Superatom. *J. Am. Chem. Soc.* **2018,** *140* (39), 12314-12317.
4. Takano, S.; Ito, S.; Tsukuda, T., Efficient and Selective Conversion of Phosphine-Protected $(MAu_8)^{2+}$ (M = Pd, Pt) Superatoms to Thiolate-Protected $(MAu_{12})^{6+}$ or Alkynyl-Protected $(MAu_{12})^{4+}$ Superatoms via Hydride Doping. *J. Am. Chem. Soc.* **2019,** *141* (40), 15994-16002.
5. Takano, S.; Ito, E.; Nakamura, T.; Tsukuda, T., Effect of Group-10 Element M (Ni, Pd, Pt) on Electronic Structure of Icosahedral $M@Au_{12}$ Cores of $MAu_{24}L_{18}$ (L = Alkynyl, Thiolate). *J. Phys. Chem. C* **2023**, 7.
6. Larriba, C.; Hogan, C. J., Free molecular collision cross section calculation methods for nanoparticles and complex ions with energy accommodation. *J. Comput. Phys.* **2013,** *251*, 344-363.
7. Larriba, C.; Hogan, C. J., Ion Mobilities in Diatomic Gases: Measurement versus Prediction with Non-Specular Scattering Models. *J. Phys. Chem. A* **2013,** *117* (19), 3887-3901.
8. Reed, A. E.; Weinstock, R. B.; Weinhold, F., Natural-Population Analysis. *J. Chem. Phys.* **1985,** *83* (2), 735-746.
9. Giles, K.; Ujma, J.; Wildgoose, J.; Pringle, S.; Richardson, K.; Langridge, D.; Green, M., A Cyclic Ion Mobility-Mass Spectrometry System. *Anal. Chem.* **2019,** *91* (13), 8564-8573.
10. Mason, E. A. M., E.W., *Transport Properties of Ions in Gases*. Wiley: New York, Chichester, Brisbane, Toronto, Singapore, 1988.
11. Smith, D. P.; Knapman, T. W.; Campuzano, I.; Malham, R. W.; Berryman, J. T.; Radford, S. E.; Ashcroft, A. E., Deciphering drift time measurements from travelling wave ion mobility spectrometry-mass spectrometry studies. *Eur. J. Mass Spectrom.* **2009,** *15* (2), 113-130.
12. Stow, S. M.; Causon, T. J.; Zheng, X. Y.; Kurulugama, R. T.; Mairinger, T.; May, J. C.; Rennie, E. E.; Baker, E. S.; Smith, R. D.; McLean, J. A.; Hann, S.; Fjeldsted, J. C., An Interlaboratory Evaluation of Drift Tube Ion Mobility-Mass Spectrometry Collision Cross Section Measurements. *Anal. Chem.* **2017,** *89* (17), 9048-9055.